Hindawi
International Journal of RF and Microwave Computer-Aided Engineering
Volume 2023, Article ID 6619073, 14 pages
https://doi.org/10.1155/2023/6619073

Research Article

Axial Ratio Improvement of Circularly Polarized Antenna Using Parasitic Elements for 5G Applications

Samira Mohammadkhani and Alireza Mallahzadeh

Electrical and Electronic Engineering Department, Shahed University, Tehran 1915713495, Iran

Correspondence should be addressed to Samira Mohammadkhani; samira.mohammadkhani@shahed.ac.ir

Received 5 July 2023; Revised 5 September 2023; Accepted 15 September 2023; Published 3 October 2023

Academic Editor: Xiao Ding

A circular polarization (CP) antenna that can switch between right-handed circular polarization (RHCP) and left-handed circular polarization (LHCP) modes has been designed and introduced for 5G applications in the 3.5 GHz frequency band in this work. The proposed antenna comprises a crossed dipole fed by a 90° hybrid coupler. The axial ratio (AR) enhancement of 190 MHz is achieved by vertically stacking a substrate with a distance of $\lambda/4$ from the ground plane, including an annular ring-shaped parasitic element above a circular-shaped disc. Consequently, by creating surface current rotation on the parasitic elements, the CP performance of the antenna is improved. According to the experiments, a wide impedance bandwidth of 930 MHz (3.19-4.12 GHz) and an overlapped AR bandwidth of 23.5% for both modes are achieved. The overall size of the antenna is $100 \times 92.5 \times 24\,\text{mm}^3$, and the gain is stable across the operating frequency band with a peak value of 6.78 dBic.

1. Introduction

With the completion of 3GPP release 15, the interest in 5G systems in industrial and commercial communications systems has significantly increased. 5G systems offer many advantages, such as faster data speeds, lower latency, improved reliability, and greater scalability. The mentioned advantages make them attractive and suitable for various applications, from the Internet of Things (IoT) to autonomous vehicles [1]. However, wideband antennas covering the sub-6 GHz NR (new radio) frequency bands like N77 (3.3-4.2 GHz) and N78 (3.3-3.8 GHz) are required when 5G bandwidth is considered for commercial applications. On the other hand, in the cellular network, ±45° slant polarizations are required for base station antennas. In contrast, dual-CP antennas exhibit a low polarization loss factor compared to conventional slant polarization antennas. Nowadays, CP antennas capable of switching between RHCP and LHCP modes are a requirement in modern telecommunication systems. Their advantages include improving the system's capacity, reducing multipath fading in wireless channels, and allowing polarization coding to be used [2]. There are two methods of achieving dual-CP performance: by using radiation structures that can generate two polarization modes or a feed network capable of providing this service [3–12]. The cooperation of four radiating arms with a reconfigurable feeding network is investigated in [3], which can selectively produce RHCP/LHCP modes by applying PIN diodes. The antenna achieved 80% impedance bandwidth and 23.5% AR bandwidth with a large volume of $150 \times 150 \times 53\,\text{mm}^3$. This structure is bulky and complicated, with a low peak gain of 4.8 dBic. Furthermore, a microstrip antenna for 5G applications is proposed in [4], which is compact with a total dimension of $30 \times 30 \times 3.2\,\text{mm}^3$ and has a dual-CP feature, but the achieved CP frequency band is narrow. The AR bandwidths of three patch

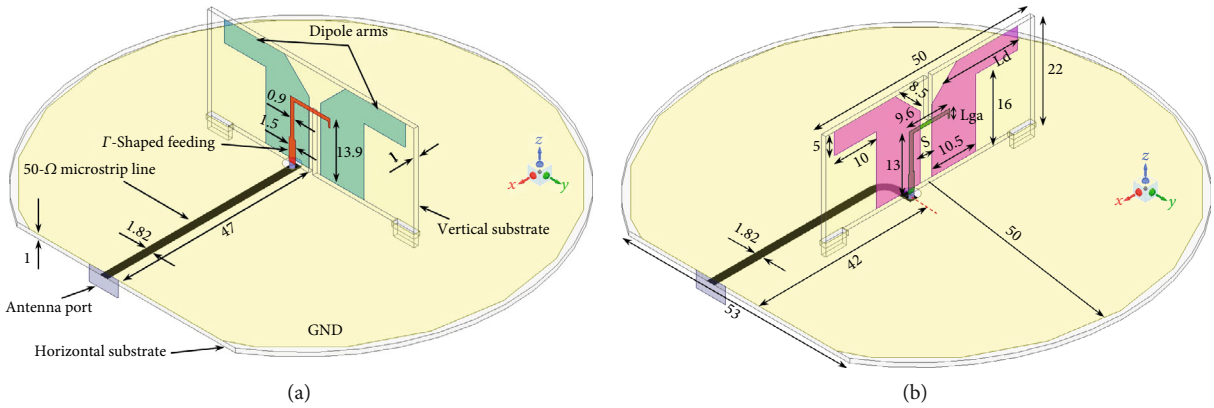

FIGURE 1: Configuration of the printed dipoles with integrated baluns: (a) dipole-1 and (b) dipole-2 (all dimensions in millimeters and $L_d = 17.5$ mm and $L_{ga} = 2$ mm).

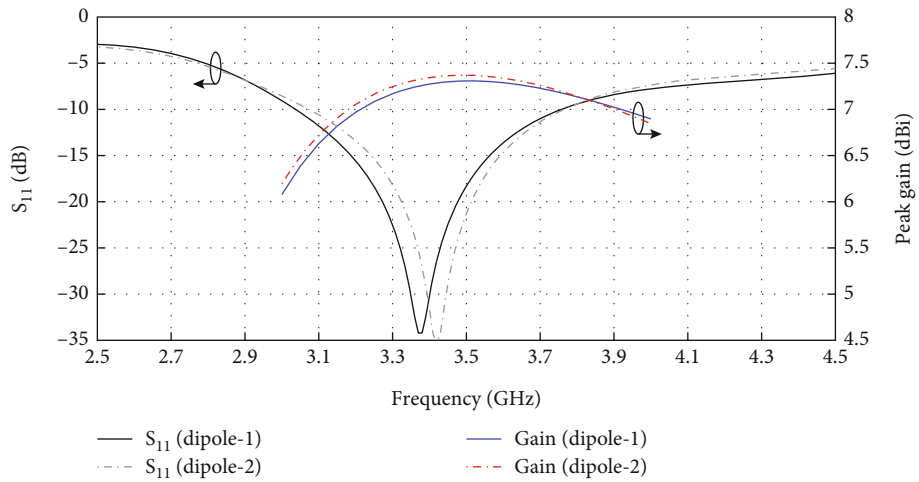

FIGURE 2: Simulated results for return loss and gain of the printed dipoles with integrated baluns.

antennas analyzed in [5–7] are narrow, with respective AR bandwidths of 8.8%, 6.1%, and 4%. A crossed-dipole antenna with phase delay lines and PIN diodes with a switchable CP mode is presented in [8], which has a compact dimension of $34 \times 31 \times 0.8\,\text{mm}^3$. This configuration achieved wide impedance bandwidth of 34% and an almost high gain of 8 dBic. However, the weakness of this design is its narrow CP bandwidth (10.2%). In [9–11], other designs of dual polarization antennas have been presented, which can be claimed to have compact dimensions, but their impedance bandwidth and circular polarization performance are not promising. On the other hand, except for [9], the rest of the mentioned designs have low gain. An RHCP/LHCP antenna with a sequential phase rotation feeding network is introduced in [12]. This design applied printed dipole antennas with integrated baluns with an overall large dimension of $85 \times 85 \times 40\,\text{mm}^3$ and low CP bandwidth of 4.3%. There are similar designs reported in [10, 13]. The integrated balun was reported in [14] for the first time. There are several advantages to using an integrated balun in dipole antenna feeding, including the following:

(1) Baluns improve signal quality by balancing the signal, thus reducing noise and interference

(2) It is possible to minimize the signal loss in the transmission line by using an integrated balun, thus improving the overall performance of the antenna

(3) When baluns are integrated into the dipole antenna, an external balun is unnecessary, and the design becomes simple with a compact size

(4) Employing balun enhances the impedance matching

(5) Also, by using balun, the impedance bandwidth of the dipole becomes wider

Integrating balun in the dipole antenna configuration is a popular choice for telecommunication services [15–18].

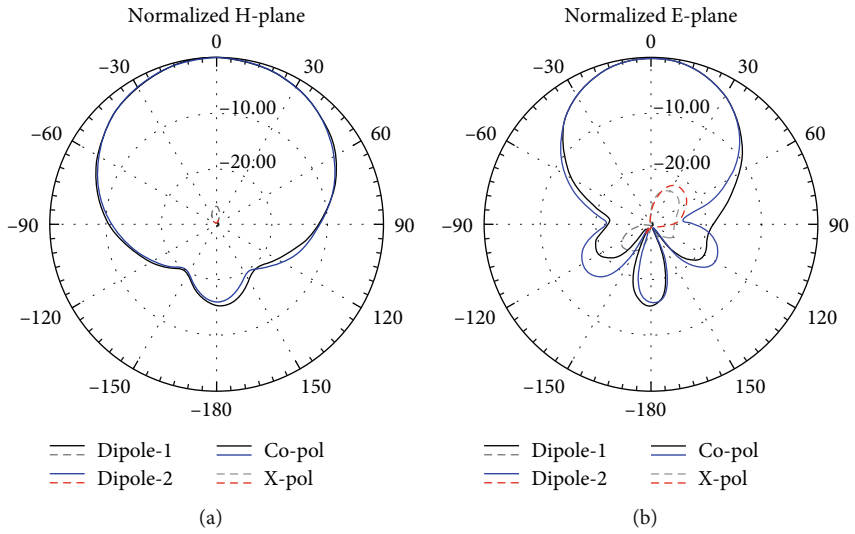

Figure 3: Simulated radiation patterns of the printed dipoles with integrated baluns: (a) H-plane and (b) E-plane.

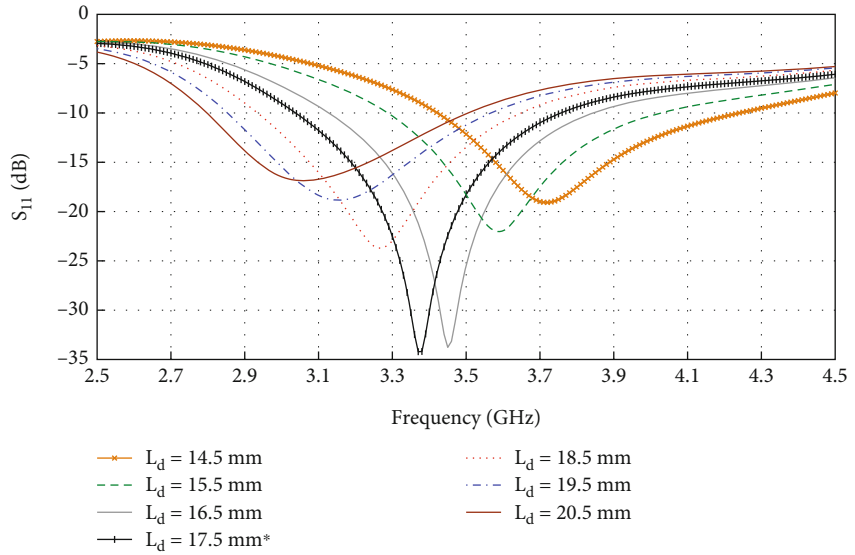

Figure 4: Effects of the dipole length L_d on the impedance bandwidth of the proposed printed dipoles with integrated baluns.

In this study, a dual-CP antenna is proposed, which is composed of printed dipoles with integrated baluns feed by a 90° hybrid coupler. A comprehensive CP operation and a wide impedance bandwidth of 25.4% are achieved by locating four pairs of annular- and disc-shaped parasitic elements above the crossed dipole. The main contribution of this work is the axial ratio enhancement of the proposed CP antenna by producing a surface current rotation on the parasitic elements.

2. Printed Dipole with Integrated Balun

This design uses two dipoles with a spatial rotation of 90° to create a crossed dipole. Figure 1 shows the configuration of dipole antennas and exhibits their physical dimensions. According to the figure, the dipole antenna is placed vertically on another substrate, including the feed line, antenna port, and ground plane. The length of the dipole arms and vertical substrate height are almost equal to the half wavelength at the impedance bandwidth central frequency in free space. In the design of both antennas, FR4 substrates with a permittivity of 4.4 and a loss tangent of 0.02 with a thickness of 1 mm have been used. Also, a portion of the horizontal substrate is cut to solder the SMA to the feed line.

From a practical point of view, the balun's function can be explained as follows: in this structure, the input signal passes through the feed line on the horizontal substrate through a small hole and a metallic pin on it to the vertical

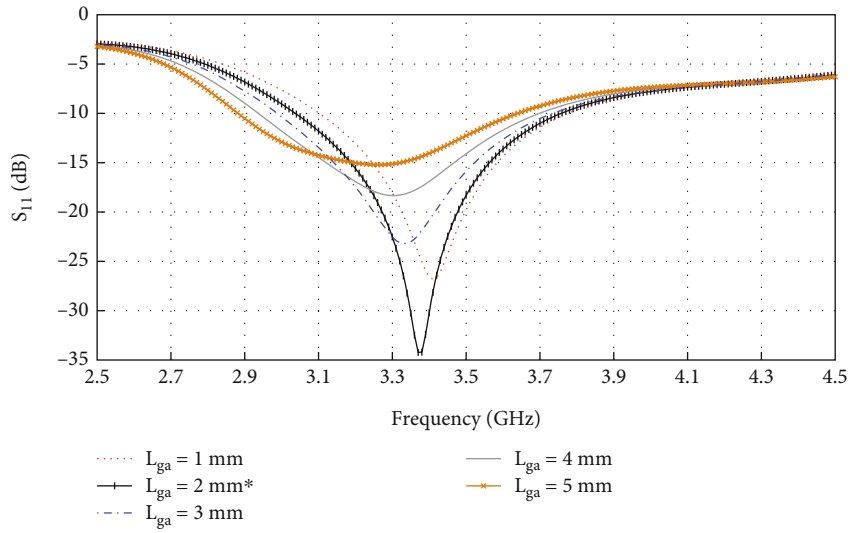

FIGURE 5: Influence of the last portion length of the Γ-feed (L_{ga}) on the impedance bandwidth of the proposed printed dipoles with integrated baluns.

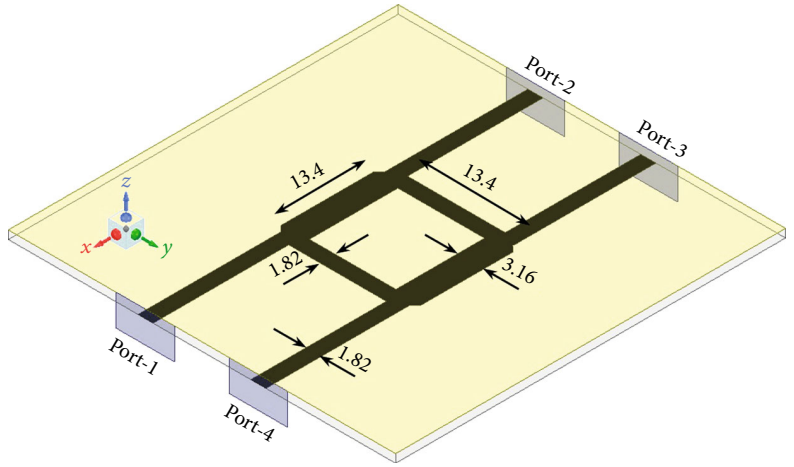

FIGURE 6: Configuration of the proposed 90° hybrid coupler (all dimensions in millimeters).

part of the Γ-shaped feed. This part acts as a microstrip line and thus delivers the input signal to the horizontal part of the Γ-shaped feed, which acts as the feed point. On the other hand, the two short-circuited vertical stubs behind the Γ-shaped feed produce a slot line. The horizontal part of the feed delivers the signal to the slot line in the form of electromagnetic coupling and through it to the dipole arms. The simulated return loss and gain results of the printed dipoles with integrated baluns are illustrated in Figure 2. The printed dipoles-1 and -2 cover the frequency bands of 3.04-3.76 GHz and 3.07-3.76 GHz, respectively. Furthermore, peak gains of 7.31 dBi for dipole-1 and 7.37 dBi for dipole-2 at the frequency of 3.5 GHz are reported.

The E- and H-planes normalized radiation patterns of the printed dipole antennas at 3.4 GHz frequency are shown in Figure 3. The antenna radiation in both planes is stable with a low cross-polarization. According to the results, half power beam widths (HPBWs) of 88.21° and 57.11° are achieved in H-plane and E-plane, respectively. In this study, the length of the dipole arms is considered almost $\lambda/4$, so a parametric study is carried out with different sizes of L_d in Figure 4. According to the parametric study, when the L_d increases from 14.5 to 20.5 mm, the center frequency of the antenna bandwidth decreases from 3.71 GHz to 3.05 GHz.

The second parametric study is done on the length of the last portion of the Γ-shaped feed. It is responsible for improving the antenna impedance matching. According to Figure 5, by changing the value of L_{ga}, the resonance intensity of the antenna varies in the central frequency. Consequently, the best value for L_{ga} is considered equal to 2 mm.

3. 90° Hybrid Coupler

Generally, in radio frequency (RF) and microwave systems, the 90° hybrid couplers are commonly used to split the

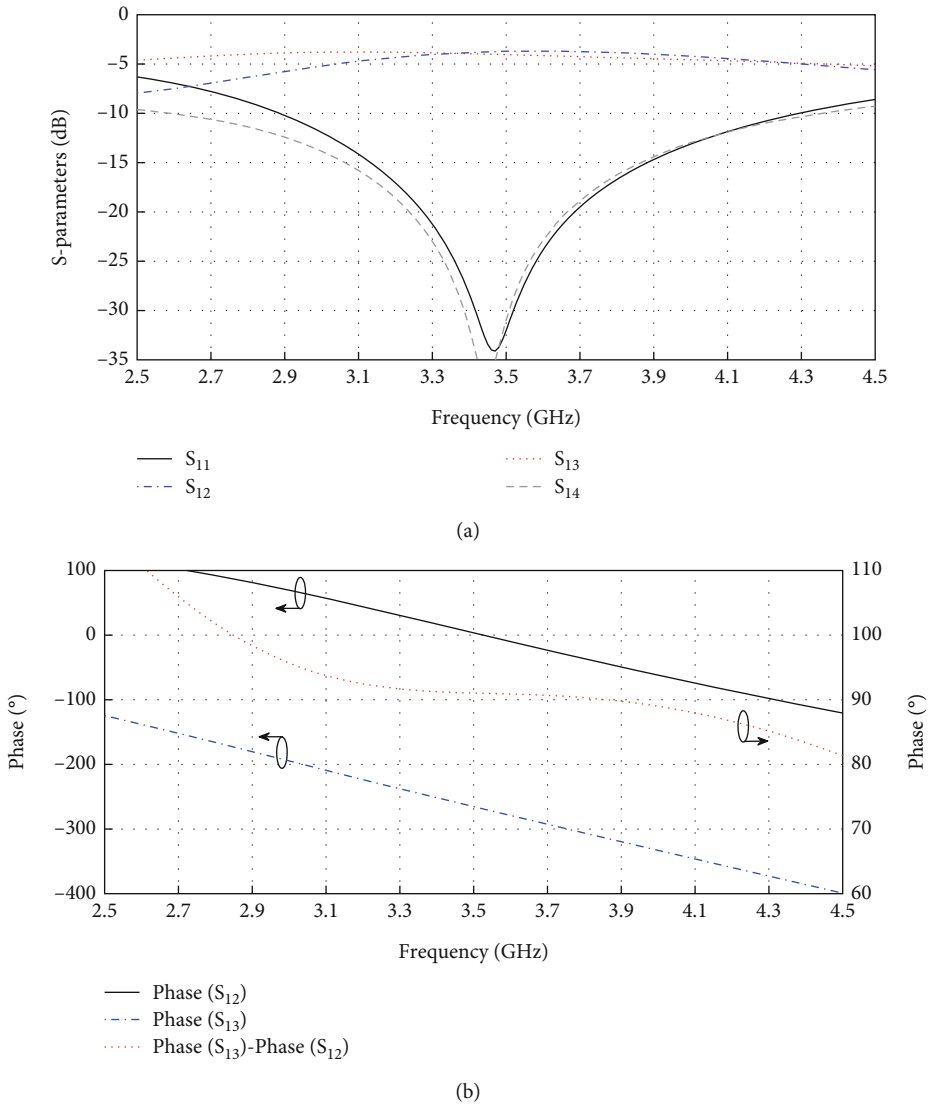

Figure 7: Simulated results for (a) S-parameters and (b) phase of the 90° hybrid coupler.

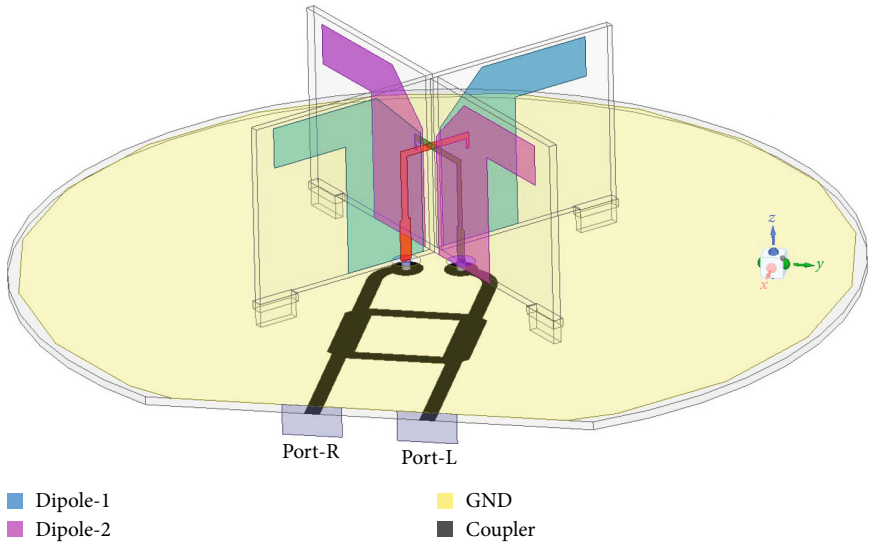

Figure 8: Configuration of the printed crossed-dipole antenna.

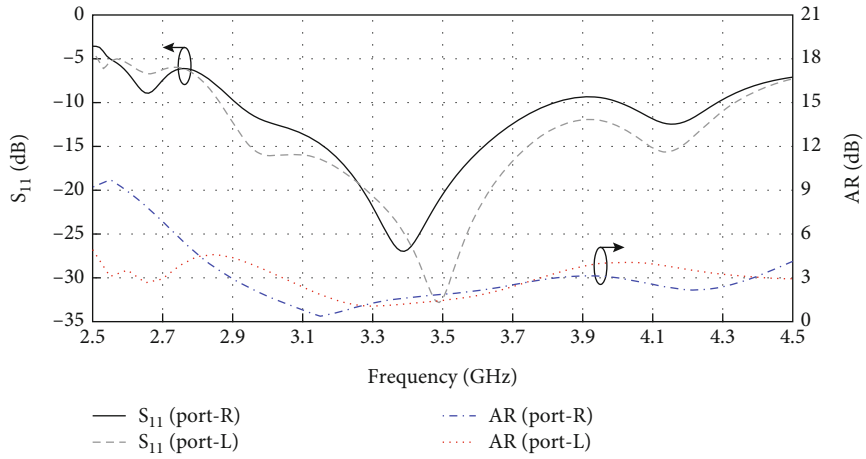

Figure 9: Simulated results for return loss and AR bandwidth of the printed crossed dipole at port-R and -L.

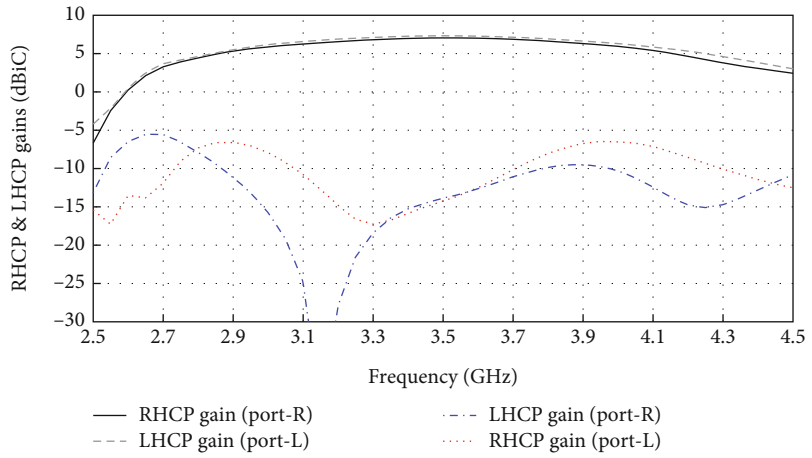

Figure 10: Simulated RHCP and LHCP gains of the printed crossed dipole at port-R and -L.

incoming signal into two equal signals with a 90° phase difference. Because of this phase difference in the outputs, it is called the quadrature coupler. Figure 6 demonstrates the configuration of the proposed 90° hybrid coupler in this work. Four ports for the coupler are named port-1, -2, -3, and -4. The input signal is applied to port-1, and the output signals are received from port-2 and -3 with the same amplitudes and 90° phase deference while a 50 Ω load terminates port-4. All dimensions are reported in the figure. Also, the introduced coupler in this section uses the same substrate as the previous section.

The results related to the proposed coupler are reported in Figure 7. Simulations approve that the presented coupler has a wide impedance bandwidth of 2.88-4.29 GHz with almost identical amplitudes in outputs. Also, the phase difference between the output signals is $90^\circ \pm 1.7^\circ$ at a frequency range of 3.3-3.8 GHz (5G systems).

4. Printed Crossed Dipole

The printed crossed-dipole antenna, fed by a 90° hybrid coupler, is shown in Figure 8. In this design, the dipoles are

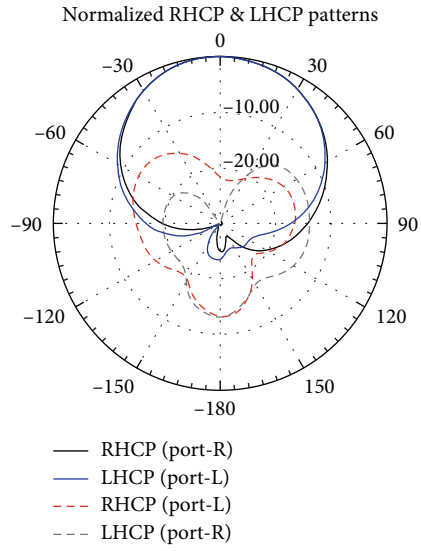

Figure 11: Simulated normalized RHCP and LHCP radiation patterns of the printed crossed dipole at the frequency of 3.2 GHz for port-R and -L.

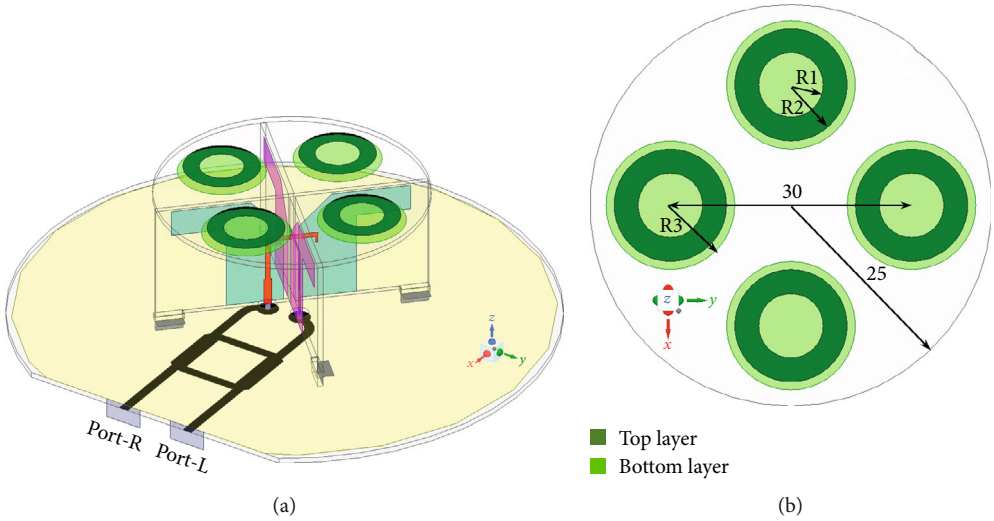

FIGURE 12: Configuration of the proposed dual-CP antenna with parasitic elements. (a) 3D view of the antenna and (b) parasitic elements (all dimensions in millimeters and $R_1 = 4$ mm, $R_2 = 7$ mm, and $R_3 = 8$ mm).

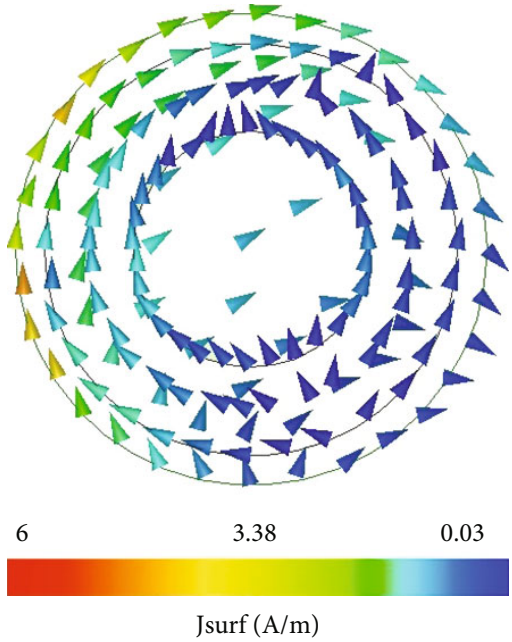

FIGURE 13: Current distribution on the annular ring- and disc-shaped parasitic elements when the port-R is excited.

placed perpendicularly to each other and then vertically positioned on the ground plane. The coupler is located under the ground plane and connected to the two ports.

The antenna ports are named port-R and port-L. When the port-R is excited, half of the signal arrives at the dipole-1 with 0° phase, and the rest is delivered to the dipole-2 with 90° phase. Consequently, RHCP radiation is achieved. On the contrary, when the port-L is excited, LHCP radiation is created. In Figures 9–11, the simulated results of the printed crossed dipole are illustrated. According to Figure 9, the impedance bandwidths of 2.91-3.82 GHz and 2.86-4.33 GHz are achieved for port-R and -L, respectively. Also, AR bandwidths of 2.89-3.83 GHz for port-R and 3.04-3.78 GHz for port-L are reported.

This design obtains peak gains of 7.05 dBic for port-R and 7.31 dBic for port-L at 3.5 GHz frequency. The RHCP and LHCP gains are plotted in Figure 10.

Moreover, the simulated normalized RHCP and LHCP radiation patterns of the printed crossed dipole at the frequency of 3.2 GHz for port-R and -L are presented in Figure 11.

The radiation patterns are stable, and using a ground plane underneath the crossed dipole generates unidirectional radiation for the antenna. The ground plane acts as a

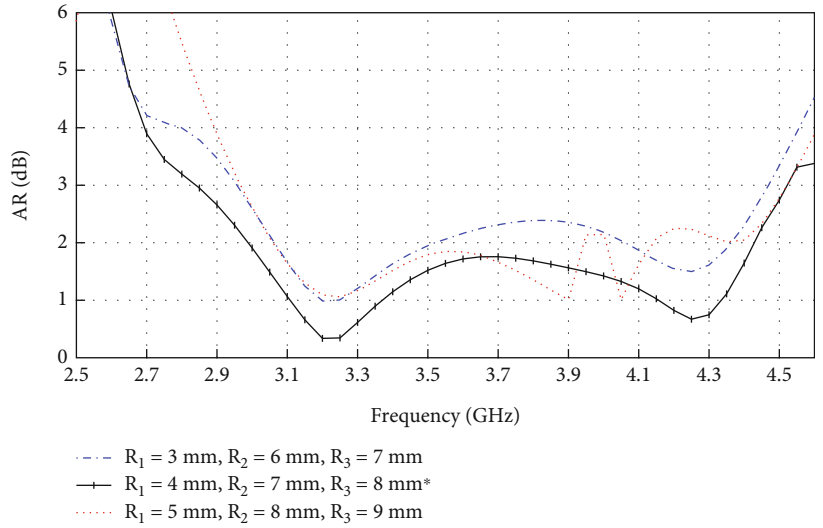

FIGURE 14: Simulated AR bandwidth of the proposed dual-CP antenna with various dimensions for parasitic elements.

metallic reflector that reflects the radiation pattern in the $+Z$ direction, producing a unidirectional pattern. Meanwhile, a crossed dipole produces stable radiation due to opposing current directions, which cancels out some radiation waves. As well, in both RHCH and LHCP modes, a 68.52° CP HPBW is achieved.

5. Proposed Dual-CP Antenna with Parasitic Elements

The proposed configuration for the CP antenna with polarization diversity is exhibited in Figure 12. The proposed CP antenna comprises a crossed dipole and four annular ring-shaped parasitic elements above four circular-shaped discs. The parasitic elements are printed on two sides of an FR4 substrate with a thickness of 1 mm and mounted on the crossed dipole. The main novelty of this study is the production of a surface current rotation on the parasitic elements in order to improve the CP performance of the proposed antenna. In this design, the parasitic elements are located in the free space between the crossed-dipoles arms.

The current distribution on the annular ring- and disc-shaped parasitic elements when the port-R is excited is plotted in Figure 13. The currents are distributed rotationally across the outer circumference of the parasitic ring and disc in a clockwise direction, which produces RHCP radiation. The rotational currents help to generate CP performance by creating a magnetic field with circularly polarized and vertical to the electric field. In this way, the electromagnetic wave radiated with circular polarization, in which the direction of the current distribution on the antenna elements determines the direction of rotation. In an ideal CP antenna, the current distribution on the antenna should follow a circular path, regardless of the actual shape of the radiating element. This circular current distribution is crucial for generating circularly polarized radiation in an annular ring element. When current flows around the annular ring, it induces a phase shift across its circumference. In a basic annular ring antenna, more than this phase shift might be required to generate proper circular polarization. Altering the geometry of the annular ring or introducing specific modifications, like using disc-shaped parasitic elements, as done in this work, can create a structure that causes the current to rotate around the ring more than once. This effectively introduces a more significant phase shift across the antenna's circumference, improving polarization purity and overall performance.

Furthermore, a parametric study is done for the different values for annular ring- and disc-shaped parasitic element dimensions in Figure 14.

The simulated and measured results of the proposed dual-CP antenna with parasitic elements are shown in Figures 15 and 16. The measured impedance bandwidths of the proposed antenna are 3.14-4.12 GHz and 3.19-4.12 GHz for port-R and -L, respectively. Furthermore, measured AR bandwidths of 2.79-4.44 GHz for port-R and 2.98-4.40 GHz for port-L are obtained. According to the experiments, the overlapped impedance bandwidth and AR bandwidth for both modes are 25.4%. Also, measured peak gains of 6.96 dBic for port-R and 6.78 dBic for port-L are reported. Notably, there has been an improvement of 190 MHz in the AR bandwidth of the proposed antenna compared to the previous section, and its gain has been reduced by 0.27 dBic.

The results confirm the improvement of the CP performance with the presence of parasitic elements. Additionally, the simulated and measured normalized RHCP and LHCP radiation patterns of the proposed dual-CP antenna with parasitic elements at the frequency of 3.2 GHz for port-R and -L are plotted in Figure 16.

Moreover, the AR values at 3.2 GHz are illustrated in Fig. 17 as a function of θ. According to the results, wide AR beamwidths of 3 dB were attained with 86.7° and 105.9°, for port-R and port-L, respectively, in $+Z$ direction.

Normalized radiation patterns of the proposed dual-CP antenna with parasitic elements for port-R and -L are

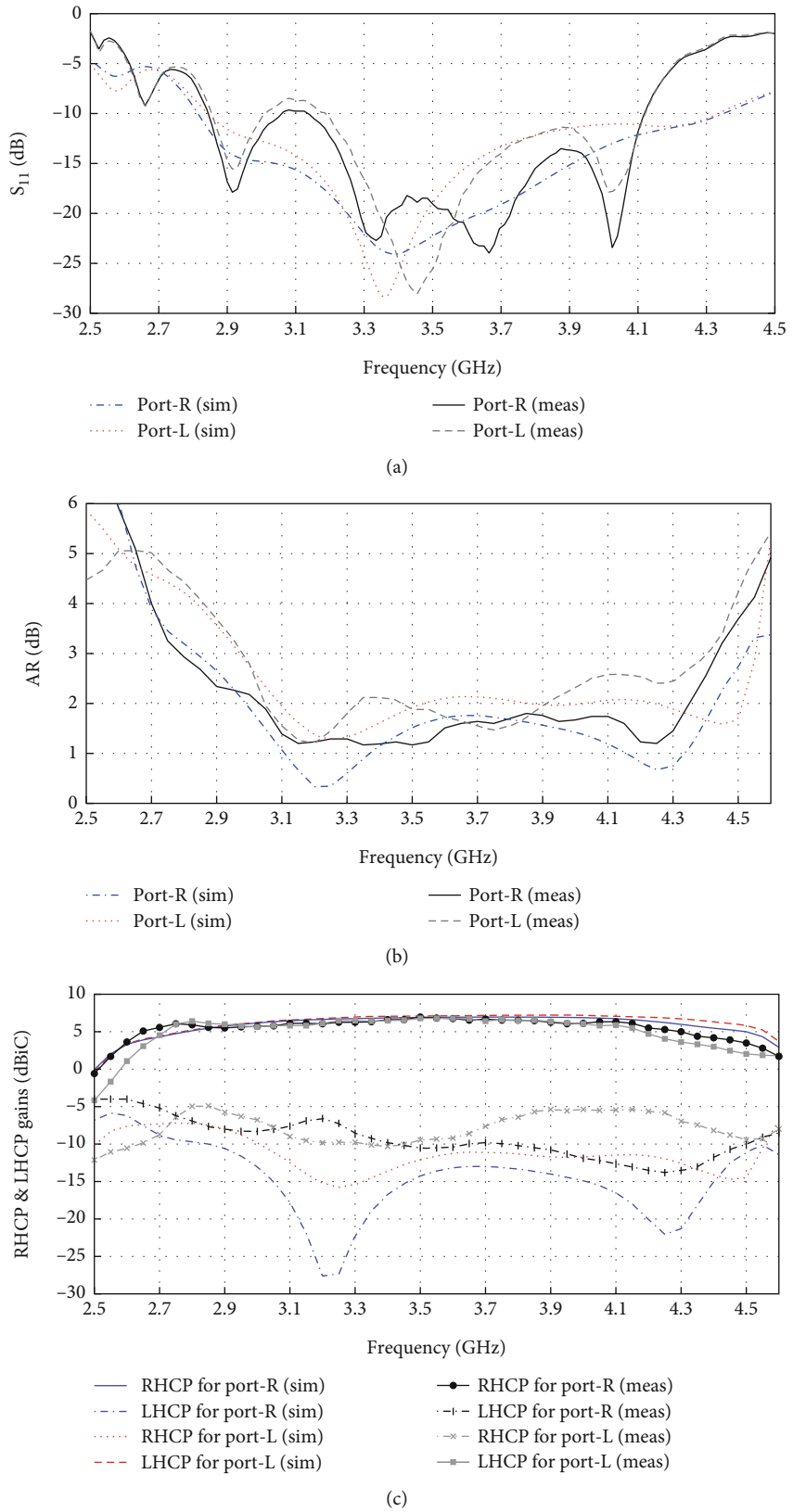

Figure 15: Simulated and measured results of the proposed dual-CP antenna with parasitic elements: (a) return loss, (b) AR bandwidth, and (c) RHCP and LHCP gains.

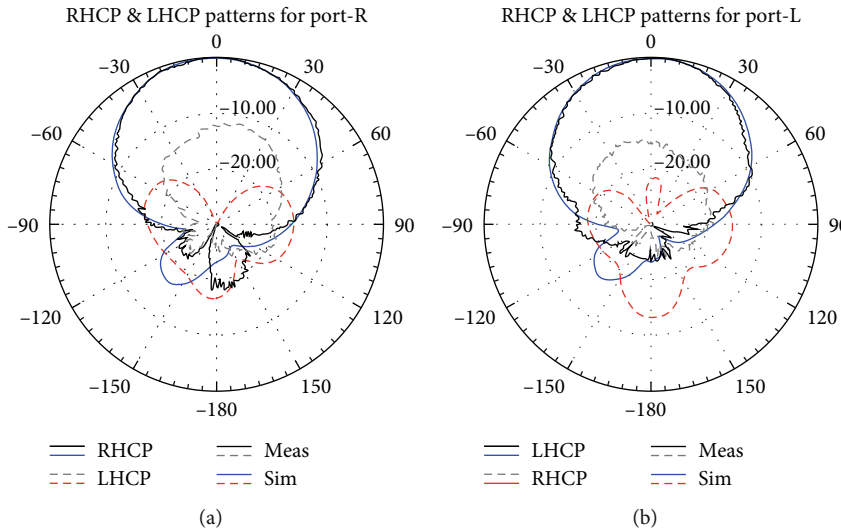

Figure 16: Simulated and measured normalized RHCP and LHCP radiation patterns of the proposed dual-CP antenna with parasitic elements at the frequency of 3.2 GHz for (a) port-R and (b) port-L.

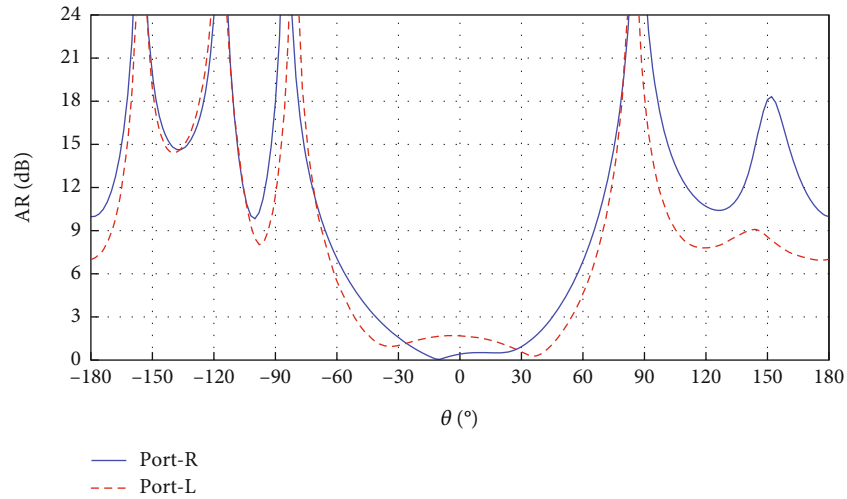

Figure 17: Simulated AR values against θ angle of the proposed dual-CP antenna with parasitic elements.

plotted in Figure 18 at different frequencies. The graphs show stable and unidirectional radiations in the entire frequency band. The HPBWs corresponding to the radiation patterns of the proposed dual-CP antenna with parasitic elements are reported in Figure 19, for different frequencies. Furthermore, the cross-polarization discrimination (XPD) graphs are calculated and plotted in Figure 20 for the proposed antenna at two ports. The XPD factor is a measure of how well an antenna can isolate its intended polarization from the orthogonal polarization. In the context of CP antennas, XPD denotes to the ability of the antenna to discriminate between its desired circular polarization and the opposite-handed circular polarization. As the XPD relates directly to the purity of circular polarization, it is a critical parameter for a circularly polarized antenna. A higher XPD value indicates a better ability to discriminate between the intended polarization and the opposite-handed polarization. As a result, CP antennas with good XPD will exhibit minimal orthogonal polarization leakage. The results indicate that the proposed antenna has peak XPD values of 33.7 dB at port-R and 21.3 dB at port-L.

Figure 21 illustrates the rotation of the electric field on an imaginary plane 45 mm above the antenna to provide a deeper understanding of the process of creating circular polarization in the proposed antenna. In this figure, port-R is activated, and the electric field at 3.2 GHz frequency is plotted in different phases. All the simulations presented in this study were obtained using HFSS ver. 15 software. The antenna proposed in this work was fabricated and tested in the antenna laboratory with high accuracy. At this stage, an Agilent E8363C network analyzer has been used to extract laboratory results. According to the measurements and simulation results, some discrepancies can be seen in some graphs, and these differences can be related to errors related to antenna manufacturing and testing procedures.

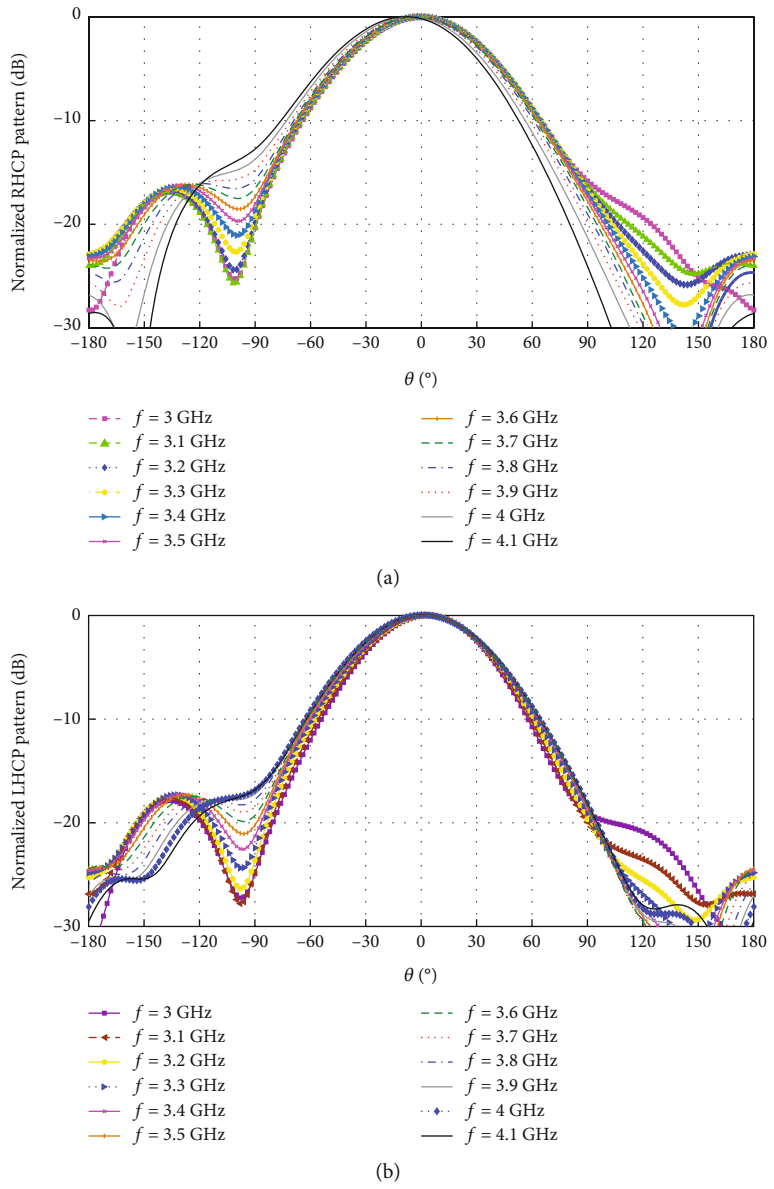

Figure 18: Normalized patterns of the proposed dual-CP antenna with parasitic elements: (a) port-R and (b) port-L.

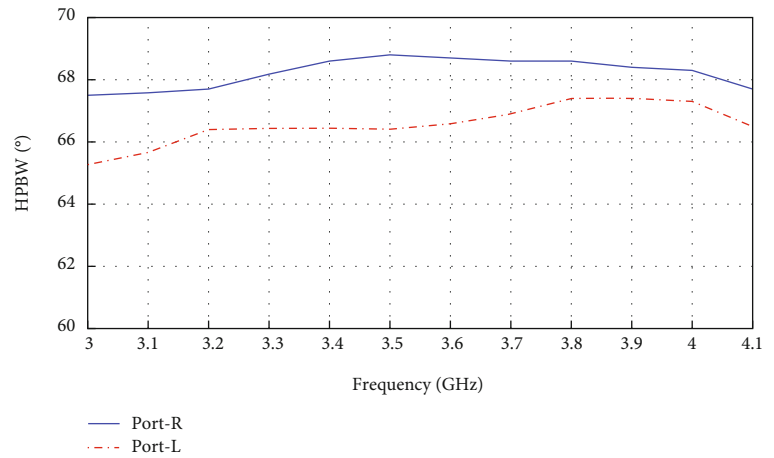

Figure 19: Simulated HPBW values against operating frequency of the proposed dual-CP antenna with parasitic elements.

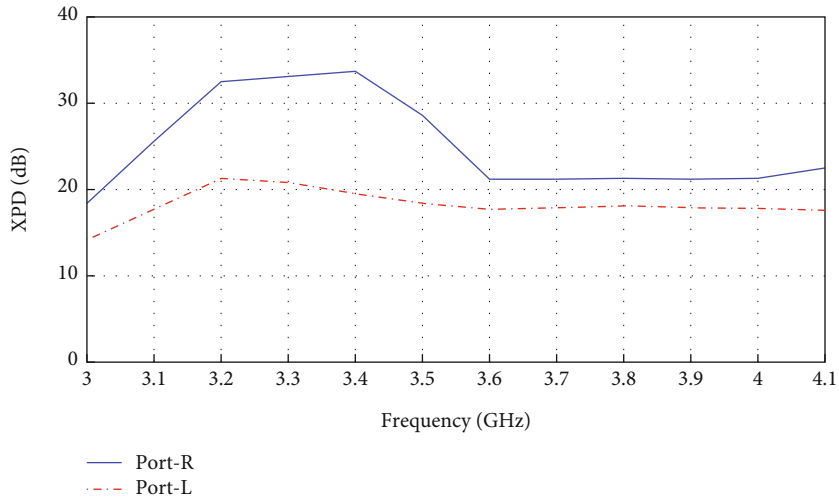

Figure 20: Simulated XPD values against operating frequency of the proposed dual-CP antenna with parasitic elements.

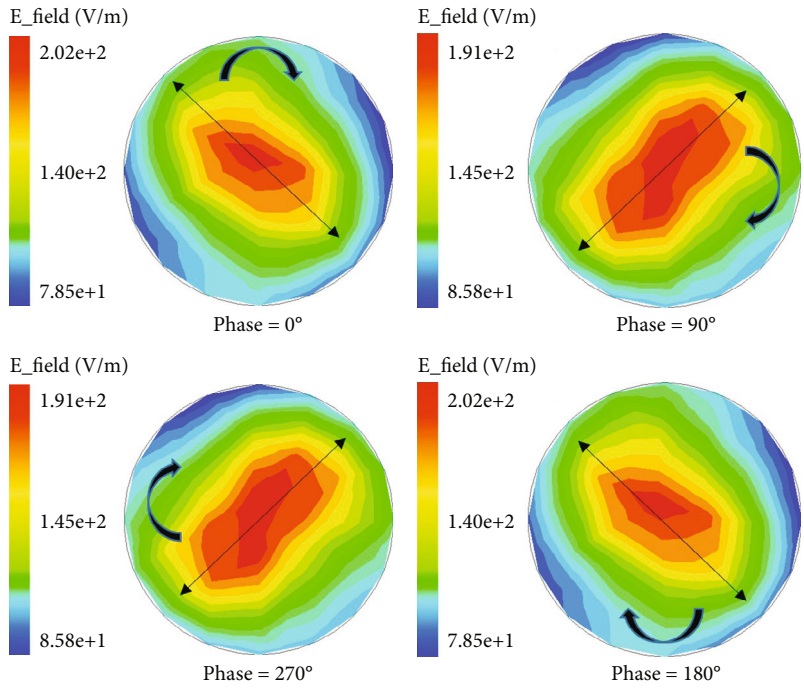

Figure 21: Simulated E-field of the proposed dual-CP antenna with parasitic elements at 3.2 GHz frequency when port-R is excited.

Figure 22: Photograph of the fabricated prototype of the proposed antenna and test setup.

A photograph of the fabricated prototype and test setup is reported in Figure 22.

As a final step, to illustrate the advantages of the proposed antenna design, its characteristics are compared with those of similar antenna designs in Table 1. Most of the articles listed in the comparison table have been thoroughly investigated in the first section of this paper. Compared to similar antennas, the design proposed in this study has better CP performance and higher gain, taking into account the dimensions of the antenna as well as the wider impedance bandwidth. Despite the compact dimensions of some antennas listed in the comparison table, they do not possess a high gain or a better CP performance.

Table 1: Comparison with state-of-the-art dual-CP antennas.

Ref.	Antenna size (mm^3)	Antenna type	Design methodology	IBW for $S11 < -10$ dB (GHz)	3 dB ARBW (GHz)	Peak gain (dBiC)	Application
[3]	$150 \times 150 \times 53$	Stacked configuration	Sequential phase rotation	1-2.35 (80%)	1.5-1.9 (23.5%)	4.8	GPS/CNSS/RFID
[4]	$30 \times 30 \times 3.2$	Microstrip antenna	Using PIN diodes	3.4-3.72 (9%)	Has a Resonance at 3.6 GHz	4.8	5G
[5]	$140 \times 80 \times 10$	Patch antenna	RF switches	2.4-2.57 (7%)	2.38-2.6 (8.8%)	8.7	WLAN
[6]	$70 \times 70 \times 10.8$	Patch antenna	Switch parasitic pins	2.29–2.69 (16%)	0.15 GHz (6.1%)	8.7	WLAN
[7]	$34 \times 31 \times 0.8$	Patch antenna	Using PIN diodes	27–29 (7.1%)	27.2-28.3 (4%)	6	5G
[8]	$34 \times 31 \times 0.8$	Printed dipoles	Sequential phase rotation	1.95-2.75 (34%)	2.05–2.27 (10.2%)	8	—
[9]	$70 \times 63.5 \times 2.2$	SIW antenna array	CP antenna elements	27.4–28.94 (5.5%)	27.7–28.8 (3.9%)	13.52	mm-wave
[10]	$40 \times 40 \times 1.6$	Printed monopoles	Mirrored image	3.4-3.8 (11.11%)	3.4-3.8 (11.11%)	5	5G
[11]	$13.7 \times 36.2 \times 15.1$	Printed monopoles	Grounded stubs	5.2-6.3 (19.13%)	5.2-6.3 (19.13%)	5.8	ISM
[12]	$85 \times 85 \times 40$	Dipole with integrated balun	Sequential phase rotation	3.3–4.2 (34.7%)	3.65–3.81 (4.3%)	9.52	5G
[13]	$150 \times 150 \times 43$	Printed dipoles	Quadrature wideband coupler	1.70–2.82 (50%)	1.70–2.82 (50%)	7.2	BTS
[10]	$40 \times 40 \times 1.6$	Printed monopoles	Elliptical-shaped resonator	3.4–3.8 (11.11)	3.4–3.8 (11.11)	5	5G
Prop.	$100 \times 92.5 \times 24$	Dipole with integrated balun	Using 90° hybrid coupler in the feed network	3.19–4.12 (25.4%)	3.19–4.12 (25.4%)	6.78	5G

6. Conclusion

This work presents a dual-CP antenna that can generate both RHCP and LHCP radiations. The proposed antenna comprises a printed crossed dipole with integrated baluns fed by a 90° hybrid coupler. In this design, a new technique is used to improve the CP performance of the antenna. In this technique, four ring-shaped parasitic elements are placed on four parasitic discs, and their set is placed on the crossed dipole. Experimental results show that using parasitic elements on the antenna increases the AR bandwidth of the antenna by 190 MHz. For the proposed antenna with parasitic elements, the overlapped impedance bandwidth and AR bandwidth for both modes are 25.4%. Compared to similar works, the presented design performs better in impedance bandwidth and circular polarization.

Data Availability

All data presented in this paper are not available anywhere else and were generated here for the first time using HFSS software.

Conflicts of Interest

The authors declare that they have no conflicts of interest.

Acknowledgments

We want to thank the Northwest Antenna and Microwave Research Laboratory (NAMRL) of Urmia University for its technical assistance.

References

[1] P. Marsh, *5G system design: architectural and functional considerations and long*, JOHN WILEY, Hoboken, NJ 07030, first edition, 2018.

[2] T. Le, H.-Y. Park, and T.-Y. Yun, "Simple reconfigurable circularly polarized antenna at three bands," *Sensors*, vol. 19, no. 10, p. 2316, 2019.

[3] W. Lin and H. Wong, "Wideband circular polarization reconfigurable antenna," *IEEE Transactions on Antennas and Propagation*, vol. 63, no. 12, pp. 5938–5944, 2015.

[4] Y. I. Al-Yasir, N. Ojaroudi Parchin, I. Elfergani et al., "A new polarization-reconfigurable antenna for 5G wireless communications," in *Lecture Notes of the Institute for Computer Sciences, Social Informatics and Telecommunications Engineering*, pp. 431–437, Springer International Publishing, 2019.

[5] A. Khidre, K.-F. Lee, F. Yang, and A. Z. Elsherbeni, "Circular polarization reconfigurable wideband E-shaped patch antenna for wireless applications," *IEEE Transactions on Antennas and Propagation*, vol. 61, no. 2, pp. 960–964, 2013.

[6] A. Khaleghi and M. Kamyab, "Reconfigurable single port antenna with circular polarization diversity," *IEEE Transactions on Antennas and Propagation*, vol. 57, no. 2, pp. 555–559, 2009.

[7] E. Al Abbas, N. Nguyen-Trong, A. T. Mobashsher, and A. M. Abbosh, "Polarization-reconfigurable antenna array for millimeter-wave 5G," *IEEE Access*, vol. 7, pp. 131214–131220, 2019.

[8] W.-S. Yoon, S.-M. Han, J.-W. Baik, S. Pyo, J. Lee, and Y.-S. Kim, "Crossed dipole antenna with switchable circular polarisation sense," *Electronics Letters*, vol. 45, no. 14, p. 717, 2009.

[9] S.-J. Park and S.-O. Park, "LHCP and RHCP substrate integrated waveguide antenna arrays for millimeter-wave applications," *IEEE Antennas and Wireless Propagation Letters*, vol. 16, pp. 601–604, 2017.

[10] S. Kumar, S. K. Palaniswamy, H. C. Choi, and K. W. Kim, "Compact dual circularly-polarized quad-element MIMO/diversity antenna for sub-6 GHz communication systems," *Sensors*, vol. 22, no. 24, p. 9827, 2022.

[11] U. Ullah, I. B. Mabrouk, and S. Koziel, "Enhanced-performance circularly polarized MIMO antenna with polarization/pattern diversity," *IEEE Access*, vol. 8, pp. 11887–11895, 2020.

[12] T. M. Cao, H. S. Vu, T. D. Bui, and M. T. Le, "Left hand and right hand circularly polarized antenna for 5G devices," in *International Conference on Industrial Networks and Intelligent Systems*, pp. 119–127, Springer International Publishing, Cham, 2021.

[13] J. -F. Li, T. Xu, D. L. Wu et al., "A dual-circularly polarized wideband dipole antenna with stable axial-ratio and half-power beamwidths," *IEEE Antennas and Wireless Propagation Letters*, vol. 22, no. 7, pp. 1701–1705, 2023.

[14] T. W. Rong Lin Li, B. Pan, L. Kyutae, J. Laskar, and M. M. Tentzeris, "Equivalent-circuit analysis of a broadband printed dipole with adjusted integrated balun and an array for base station applications," *IEEE Transactions on Antennas and Propagation*, vol. 57, no. 7, pp. 2180–2184, 2009.

[15] M. H. Teimouri, C. Ghobadi, J. Nourinia, K. Kaboutari, M. Shokri, and B. S. Virdee, "Broadband printed dipole antenna with integrated balun and tuning element for DTV application," *AEU - International Journal of Electronics and Communications*, vol. 148, article 154161, 2022.

[16] R. Nasirzade, J. Nourinia, C. Ghobadi, M. Shokri, and R. Naderali, "Broadband printed MIMO dipole antenna for 2.4 GHz WLAN applications," *Journal of Instrumentation*, vol. 15, no. 1, 2020.

[17] A. Hatamian, C. Ghobadi, J. Nourinia, and M. Shokri, "A compact triple-band printed dipole antenna using C-shaped resonators with stable radiation for GSM/ism/WLAN applications," *Microwave and Optical Technology Letters*, vol. 65, no. 2, pp. 611–618, 2023.

[18] M. Shokri, P. Faeghi, K. Kaboutari et al., "A printed dipole antenna for WLAN applications with anti-interference functionality," in *2021 Photonics & Electromagnetics Research Symposium (PIERS)*, Hangzhou, China, 2021.